Nanoscale Research Letters
a SpringerOpen Journal

NANO EXPRESS Open Access

Efficient p-type dye-sensitized solar cells with all-nano-electrodes: $NiCo_2S_4$ mesoporous nanosheet counter electrodes directly converted from $NiCo_2O_4$ photocathodes

Zhiwei Shi[1], Hao Lu[1], Qiong Liu[1], Fengren Cao[1], Jun Guo[2], Kaimo Deng[1] and Liang Li[1*]

Abstract

We report the successful growth of $NiCo_2S_4$ nanosheet films converted from $NiCo_2O_4$ nanosheet films on fluorine-doped tin oxide substrates by a low-temperature solution process. Low-cost $NiCo_2S_4$ and $NiCo_2O_4$ nanosheet films were directly used for replacing conventional Pt and NiO as counter electrodes and photocathodes, respectively, to construct all-nano p-type dye-sensitized solar cells (p-DSSCs) with high performance. Compared to Pt, $NiCo_2S_4$ showed higher catalytic activity towards the I^-/I_3^- redox in electrolyte, resulting in an improved photocurrent density up to 2.989 mA/cm^2, which is the highest value in reported p-DSSCs. Present p-DSSCs demonstrated a cell efficiency of 0.248 % that is also comparable with typical NiO-based p-DSSCs.

Keywords: Dye-sensitized solar cells; p-type; Counter electrodes; Nanosheets; Ternary sulfides

Background

Dye-sensitized solar cells (DSSCs) are typically composed of dye-sensitized nanocrystalline semiconductors, an iodide/triiodide (I^-/I_3^-) redox electrolyte, and a counter electrode (CE) [1-3]. One research direction to improve conversion efficiency of DSSCs is to construct a tandem DSSC in a sandwich configuration, which combines a photoanode from an n-type DSSC (n-DSSC) and a photocathode from a p-type DSSC (p-DSSC) [4,5]. In a tandem cell, the overall photovoltage is the sum of two parts, while the photocurrent is limited by the photoelectrode with a smaller current. Recently, the conversion efficiency of n-DSSCs reaches as high as 12% [6], but the p-DSSCs still suffers from low efficiencies and thus limit the overall efficiency of the tandem DSSCs. Although much attention has been paid to search ideal p-type semiconductor materials and efficient dyes [7-10], the best p-DSSC exhibits efficiency of only 1.3% by utilizing $[Co(en)_3]^{2+/3+}$ redox couple and PMI-6 T-TPA dye [11]. It is worthy to note that few results are devoted to the study of CEs for p-DSSCs, ignoring a feasible approach to further improve the conversion efficiency. The function of CEs is to transfer the electrons (holes) arriving from the external circuit to the redox electrolyte to catalyze the reduction (oxidization) of the redox couple. Generally, platinum (Pt) is the preferred CE material due to its superior electrocatalytic activity, high electrical conductivity, and excellent chemical stability. However, as a noble metal, Pt is one of the most expensive materials and has low abundance in the earth, preventing it from being used for large-scale manufacture of DSSCs.

Since Grätzel's group found that cobalt sulfide (CoS) has excellent catalytic activity for the iodine-based redox couples [12], great efforts have been made to exploit abundant low-cost substitutes for Pt, including metal sulfides, nitrides, and carbides [13-16] Unfortunately, to date, these reported catalysts can hardly compete with Pt in the performance of DSSCs. As an important class of chalcogenides, semiconducting sulfides have drawn intensive attention due to their distinctive electronic properties, interesting chemical behaviors, and a variety of applications. Particularly, binary metal sulfides (NiS and CoS) have exhibited almost the same conversion

* Correspondence: lli@suda.edu.cn
[1]College of Physics, Optoelectronics and Energy & Collaborative Innovation Center of Suzhou Nano Science and Technology, Soochow University, Suzhou 215006, People's Republic of China
Full list of author information is available at the end of the article

efficiency as Pt in DSSCs [17-19]. Compared with binary NiS and CoS, ternary sulfide $NiCo_2S_4$ is expected to offer richer redox reactions due to the contributions from both nickel and cobalt ions. For example, $NiCo_2S_4$ has demonstrated enhanced catalytic activity for oxygen evolution and polysulfide redox couple [20,21]. Recent results also showed that $NiCo_2S_4$ can be used as CEs of n-type DSSCs, but its efficiencies are lower than those of the Pt-based cells [22,23].

In this paper, we reported low-cost $NiCo_2S_4$ nanosheet (NS) films grown on a fluorine-doped tin oxide (FTO) substrate as a high-performance CE for p-DSSCs composed of p-type $NiCo_2O_4$ semiconductor photocathode. The $NiCo_2S_4$ NS film was synthesized via a facile two-step process including the synthesis of $NiCo_2O_4$ NS film on a FTO substrate and then an anion ion exchange process under hydrothermal reaction. When applying the $NiCo_2S_4$ as a CE and $NiCo_2O_4$ as a photocathode, novel all-nano-p-DSSCs achieved an impressive photocurrent of 2.989 mA/cm^2 and cell efficiency of 0.248% versus 1.824 mA/cm^2 and 0.158% for Pt under the same conditions. To the best of our knowledge, this efficiency is comparable and even higher than that of NiO-based p-DSSCs with an I^-/I^{3-} redox couple.

Methods

Synthesis of $NiCo_2S_4$ nanosheet films

A two-step hydrothermal process was used to synthesize $NiCo_2S_4$ nanosheet films on FTO substrates. In the first step, $NiCo_2O_4$ nanosheet arrays were synthesized by a modified low-temperature hydrothermal method [24-28]. Typically, 30 mmol of urea and 8 mmol of NH_4F were dissolved completely in 30 mL deionized water, followed by the addition of 1 mmol of $Ni(NO_3)_2 \cdot 6H_2O$ and 2 mmol of $Co(NO_3)_2 \cdot 6H_2O$. The mixture was transferred to a capped bottle with a FTO growth substrate facing down in the precursor at 85°C for 6 h. Once the reaction was finished, the samples were rinsed with deionized water and treated in air at 350°C for 3 h, and the $NiCo_2O_4$ nanosheet films were obtained. In the second step, to synthesize $NiCo_2S_4$ nanosheet films, the $NiCo_2O_4$ nanosheet films were put into $Na_2S \cdot 9H_2O$ solution (2 mol/L) and reacted in an autoclave at 160°C for 10 h. After the reaction, the samples were rinsed thoroughly with deionized water and dried at 60°C for 5 h in a vacuum oven.

Fabrication of p-DSSC devices

The photocathode was prepared by immersing a $NiCo_2O_4$ sample in an ethanol solution containing 0.5 mM of N719 dye (cis-bis(isothiocyanato)bis(2,2′-bipyridyl-4,4′-dicarboxylic acid)ruthenium(II)) (Solaronix SA, Aubonne, Switzerland) for 3 h, followed by rinsing in ethanol to remove dye absorbed physically, and drying in air. The Pt counter electrode was prepared by spin coating 1 mM of chloroplatinic acid ($H_2PtCl_6 \cdot 6H_2O$, Aldrich, 99.9%) in 2-propanol (Sigma-Aldrich, St. Louis, MO, USA; 99.7%) onto a FTO substrate and then heating at 350°C for 30 min. The as-prepared $NiCo_2S_4$ nanosheet films were used directly as counter electrodes. The dye-coated photocathodes were sealed against Pt or $NiCo_2S_4$ counter electrodes with hot melt plastic spacers (Solaronix, 60-μm thick). The electrolyte (0.1 M LiI, 0.03 M I_2, 0.5 M tetrabutylammonium iodide, and 0.5 M 4-tert-butylpyridine in acetonitrile) was introduced into the gap between two electrodes by a syringe. The active area of DSSCs was 0.2 cm^2.

Materials characterization

The morphology was characterized by field emission scanning electron microscope (FESEM; Hitachi SU8010, Hitachi Ltd., Tokyo, Japan). The microstructure was analyzed by high-resolution transmission electron microscopy (HRTEM) with selected area electron diffraction (SAED) (FEI Tecnai G2 F20 S-TWIN TMP, FEI, Hillsboro, OR, USA). The phase of products was checked by an X-ray diffractometer (XRD).

Device measurements

Photocurrent-voltage (*J-V*) characteristics were performed using a Keithley 2400 SourceMeter (Keithley Instruments Inc., Cleveland, OH, USA) under simulated AM 1.5G illumination (100 mW/cm^2) provided by a solar light simulator (94043A, Newport Corp., Irvine, CA, USA). Cyclic voltammetry (CV) and the electrochemical impedance spectroscopy (EIS) were measured with an Autolab electrochemical workstation (PGSTAT 302 N, Metrohm AG, Utrecht, The Netherlands). CV was carried out in a three-electrode system with different counter electrodes as working electrodes, a Pt foil as counter electrode, and a Ag/Ag^+ electrode as reference electrode at a scan rate of 50 mV/s. The electrodes were immersed into an anhydrous acetonitrile solution containing 0.1 M $LiClO_4$, 10 mM LiI, and 1 mM I_2. EIS was actualized with a symmetric cell assembled with two identical counter electrodes at open-circuit voltage (V_{oc}) bias under dark condition. The measured frequency ranged from 10 mHz to 1 MHz and the magnitude of the alternative signal was 10 mV.

Results and discussion

Figure 1a shows the XRD pattern of the samples after conversion process. All of the diffraction peaks can be indexed to $NiCo_2S_4$ (JCPDF card no. 43–1477). Before the ion exchange process, the diffraction peaks come from $NiCo_2O_4$ (Additional file 1: Figure S1). Figure 1b,c,d depicts typical scanning electron microscopy (SEM) images of the $NiCo_2S_4$ nanosheets. A low-magnification SEM image in Figure 1b shows a large-scale and uniform

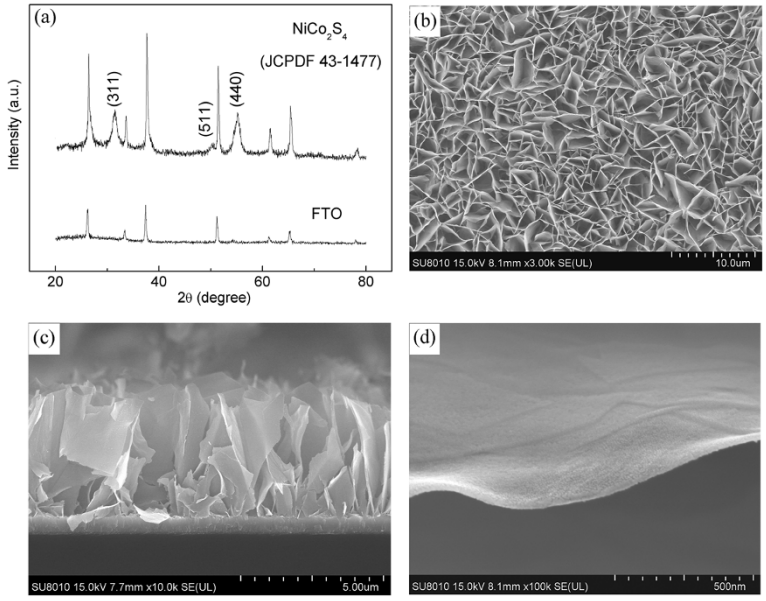

Figure 1 XRD pattern and SEM images of a sample. (a) XRD pattern of $NiCo_2S_4$ nanosheet films and representative SEM images of **(b)** large-scale and uniform growth, **(c)** cross section, and **(d)** sheet-like and porous character.

nanosheet array, and the corresponding cross-sectional image (Figure 1c) indicates that the nanosheets are vertically grown and have close contact with the FTO substrate. Higher-magnification image in Figure 1d further confirms the sheet-like character. Compared to the $NiCo_2O_4$ nanosheets (Additional file 1: Figure S2), the morphology of $NiCo_2S_4$ is almost the same and the porous surface is preserved.

The microstructure of the nanosheets is revealed by HRTEM images, as shown in Figure 2. Figure 2a,b shows that mesopores are distributed throughout the whole surface of the nanosheets. The size of the mesopores is evaluated by measuring the N_2 adsorption-desorption curve (Figure 2c). The Brunauer-Emmett-Teller (BET) surface area of $NiCo_2S_4$ nanosheets is as high as 28.5 cm^3/g. The pore-size distribution analysis (the inset in Figure 2c) gives an average pore size of 14.6 nm. The lattice fringes and corresponding SAED pattern (Figure 2d) indicate the polycrystalline nature of these nanosheets, and the diffraction rings can be indexed to the (111), (220), (311), (400), and (440) planes of the $NiCo_2S_4$ phase, which is consistent with the XRD result.

To characterize the electrocatalytic activity of $NiCo_2S_4$ NS and Pt catalysts, CV experiments were carried out in a three-electrode system, as shown in Figure 3a. The redox reactions can be expressed by Equations 1 and 2 [29].

$$3I^- \rightarrow I_3^- + 2e^- (\text{oxidation, anodic peak}) \quad (1)$$

$$I_3^- + 2e^- \rightarrow 3I^- (\text{reduction, cathodic peak}) \quad (2)$$

In the CV curves, the peak-to-peak separation (E_{pp}) and the peak current density are two important parameters for comparing catalytic performance of different CEs [30]. The anodic current density is generally related with the rate of reaction for I^- oxidation in p-DSSCs. Compared to Pt CE, the $NiCo_2S_4$ NS CE possesses higher anodic and cathodic current densities, indicating that $NiCo_2S_4$ NS has higher catalytic activity than Pt. In addition, the E_{pp} value is inversely correlated with the standard electrochemical rate constant of a redox reaction. The E_{pp} of the $NiCo_2S_4$ NS CE is 0.420 V, which is almost similar with that (0.408 V) of the Pt CE. Enhanced current density and similar E_{pp} imply that the performance of $NiCo_2S_4$ NS CE is comparable to and even better than that of Pt CE.

EIS is a powerful tool to reveal the inherent electrochemical behaviors and the interfacial charge transfer process [31]. To further evaluate the catalytic activities of $NiCo_2S_4$ NS and Pt CEs, EIS experiments were performed using symmetric cells fabricated with two identical electrodes (CE/electrolyte/CE), as shown in Figure 3b. The Nyquist plots show two semicircles in the high-frequency (left) and low-frequency (right) regions. According to the equivalent circuit model (the inset of Figure 3b) [32,33], the high-frequency intercept on the real axis represents the ohmic series resistance (R_s) outside a circuit (substrate resistance and lead connection), and the semicircle arises from the charge-transfer resistance (R_{ct}) at the CE/electrolyte interface and the corresponding phase angle element (CPE). The low-frequency region results from the

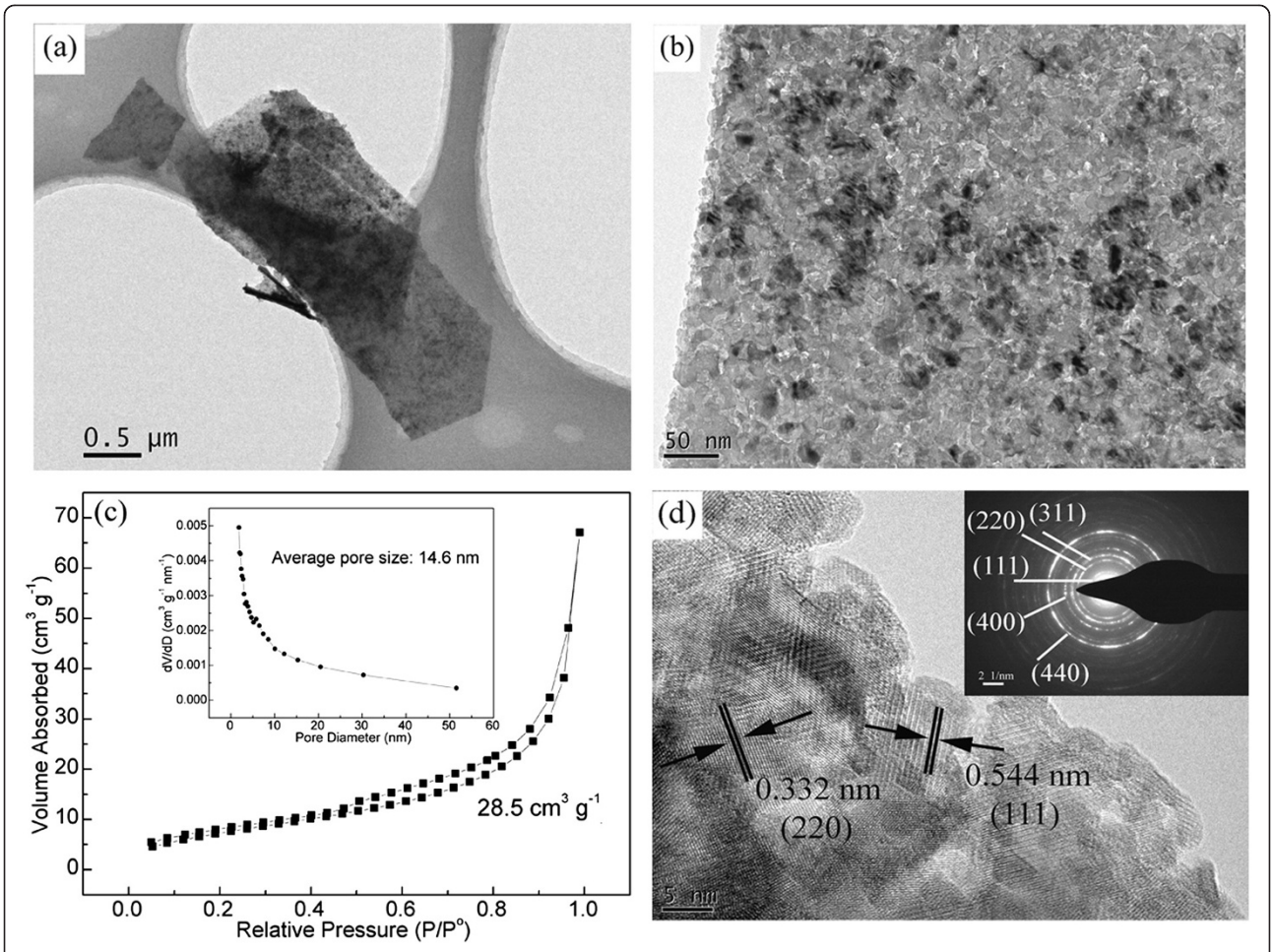

Figure 2 Microstructure of the nanosheets. (a, b) TEM images of nanosheet films, indicating that nanosheets are composed of mesopores. **(c)** N_2 adsorption-desorption and pore-size distribution curves. **(d)** Lattice fringes and SAED pattern (inset) of the nanosheet.

Nernst diffusion impedance (Z_N) of the redox couple in the electrolyte. These parameters were obtained by fitting the Nyquist plots with the Autolab NOVA software, and corresponding results are listed in Table 1. The value of R_s for $NiCo_2S_4$ NS is almost the same with that for Pt, because the preparation procedure of two electrodes is similar. The R_{ct} value for $NiCo_2S_4$ NS CE is 1.25 Ω cm^2, which is lower than that for Pt (7.32 Ω cm^2), indicating that the former has much higher catalytic activity than the latter as evidenced by the CV tests. The value of Z_N can be calculated using Equation 3 [34]:

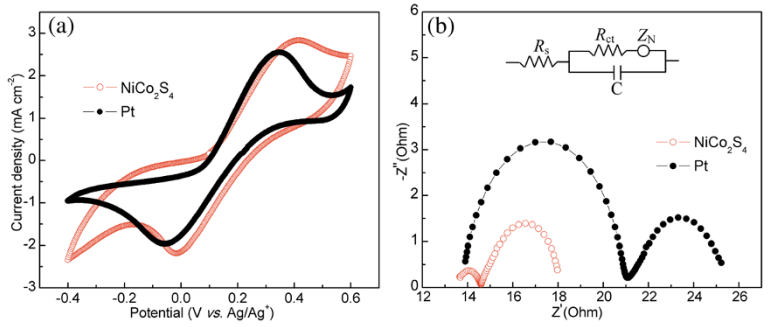

Figure 3 CV curves and Nyquist plots. (a) CV curves for the $NiCo_2S_4$ nanosheet and Pt-based counter electrodes. **(b)** Nyquist plots of EIS for symmetric cells assembled with two identical counter electrodes at an open-circuit voltage bias under dark condition.

Table 1 Detailed photovoltaic and EIS parameters of the DSSCs with counter electrodes composed of $NiCo_2S_4$ nanosheets and Pt

Counter electrons	J_{sc} (mA/cm^2)	V_{oc} (V)	FF	η (%)	R_s (Ω cm^2)	R_{ct} (Ω cm^2)	Z_N (Ω cm^2)
Pt	1.824	0.1459	59.4	0.158	13.8	7.32	4.44
$NiCo_2S_4$	2.989	0.1486	55.8	0.248	13.4	1.25	3.58

$$Z_N = \frac{kT}{n^2 e_0{}^2 cA\sqrt{i\omega D}} \tanh\left(\sqrt{\frac{i\omega}{D}}\delta\right), \quad (3)$$

where k is the Boltzmann constant, T is the absolute temperature, n is the number of holes involved in the electrochemical oxidation of I^- at the electrode, e_0 is the elementary charge, c is the concentration of I^-, A is the electrode area, ω is the angular frequency, D is the diffusion coefficient of I^-, and δ is the thickness of the diffusion layer. The Z_N values for $NiCo_2S_4$ and Pt CEs are 3.58 and 4.44 Ω cm^2, respectively, indicating that the D of I^- in the $NiCo_2S_4$ cell is larger than that in the Pt cell. For the same electrolyte, a larger D means that the electrode has higher electrocatalytic activity, because faster oxidation of the I^- on the surface of catalysts can accelerate the diffusion of I^- ions in electrolyte.

Figure 4 shows the *J-V* curves of the DSSCs with $NiCo_2S_4$ NS and Pt CEs at 1-sun (AM 1.5G, 100 mW/cm^2) illumination. The detailed photovoltaic parameters, including V_{oc}, short-circuit current density (J_{sc}), fill factor (FF), and cell efficiency (η) are summarized in Table 1. The DSSC with a $NiCo_2S_4$ NS CE produces an excellent cell efficiency of 0.248%, which is higher than that (0.158%) for the Pt-based reference cell. It is worthy to note that present efficiency is comparable and even higher than reported results for p-DSSCs based on typical NiO and other materials, as shown in Additional file 1: Tables S1. The V_{oc} value of a p-DSSC is determined by the difference between the Fermi level in the photocathode and the redox potential of I^-/I^{3-}. In the present study, there is no change in the photocathodes and the redox electrolyte; thus, the V_{oc} values of the DSSCs based on $NiCo_2S_4$ and Pt CEs remain almost the same. FF is mainly affected by the electron back transfer and charge recombination within devices, and series resistance, etc. Although the FF of $NiCo_2S_4$ CEs is a little lower than that of Pt CEs, the J_{sc} of $NiCo_2S_4$ CEs is much higher than that of Pt CEs, resulting in a higher η. The improved J_{sc} of $NiCo_2S_4$-based cell is ascribed to its mesoporous structure, which not only provides large active surface area for I^- oxidation but also constructs lots of open channels to facilitate the diffusion of I^-/I^{3-} redox species. Both enhanced catalytic reaction and high diffusion rate accelerate the transfer of photogenerated holes and thus an increased current density can be expected.

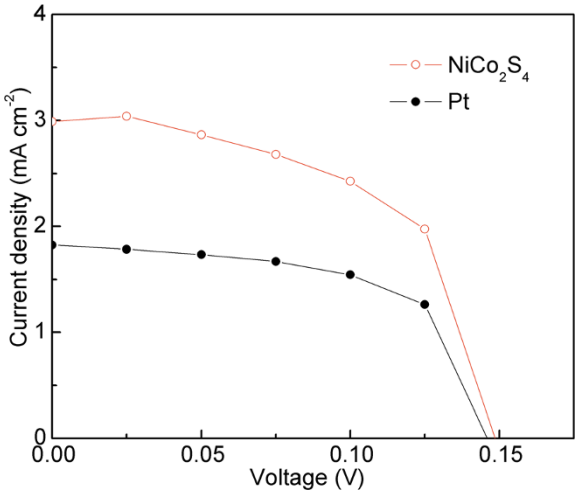

Figure 4 *J-V* curves of the DSSCs with $NiCo_2S_4$ NS and Pt CEs at 1-sun illumination. *J-V* characteristics of DSSCs with the $NiCo_2S_4$ nanosheet and Pt as counter electrodes, and the $NiCo_2O_4$ nanosheet as a photocathode.

Conclusions

Low-cost $NiCo_2S_4$ NS films with high catalytic activity have been utilized as CEs of p-DSSCs based on $NiCo_2O_4$ NS photocathodes. The mesoporous nanosheets provide a large catalytically active area and facilitate the transport of I^-/I_3^- redox in electrolyte. The DSSCs with $NiCo_2S_4$ as a CE produce a higher J_{sc} and η (2.989 mA/cm^2 and 0.248%, respectively) than those (1.824 mA/cm^2 and 0.158%, respectively) of the cell with a Pt CE. This J_{sc} can almost match the performance of p-DSSCs, but the V_{oc} is still low. In the future, improving the V_{oc} by doping materials and replacing electrolyte types is an important route. The use of cost-effective $NiCo_2S_4$ as an alternative to noble Pt, in combination with a facile fabrication method, may pave the way for low-cost, scalable, and high-efficiency DSSCs.

Additional file

Additional file 1: Supporting information. This file contains XRD pattern and SEM images of $NiCo_2O_4$ nanosheets and comparison of photovoltaic parameters for the present and previously reported p-DSSCs.

Competing interests
The authors declare that they have no competing interests.

Authors' contributions

ZS participated in the design of experiments and drafted the manuscript. HL participated in the IV analysis and revision of the manuscript. QL participated in the analysis of the CV data. FC participated in the experiment of the XRD measurements and data analysis. JG participated in the measurements and analysis of TEM. KD participated in the collection of SEM. LL participated in the design and analysis of data and revision of the manuscript. All authors read and approved the final manuscript.

Acknowledgements

We acknowledge the support from the National Natural Science Foundation (51422206, 51372159, 11304217), 1000 Youth Talents Plan, and Jiangsu Shuangchuang Plan, a project supported by Jiangsu Scientific and Technology Committee for Distinguished Young Scholars (BK20140009) and funded by the Priority Academic Program Development of Jiangsu Higher Education Institutions (PAPD).

Author details

[1]College of Physics, Optoelectronics and Energy & Collaborative Innovation Center of Suzhou Nano Science and Technology, Soochow University, Suzhou 215006, People's Republic of China. [2]Analysis and Testing Center, Soochow University, Suzhou 215006, People's Republic of China.

Received: 10 August 2014 Accepted: 23 September 2014
Published: 11 November 2014

References

1. Hagfeldt A, Boschloo G, Sun L, Kloo L, Pettersson H: **Dye-sensitized solar cells.** *Chem Rev* 2010, **110:**6595.
2. Zhang QF, Dandeneau CS, Zhou XY, Cao GZ: **ZnO nanostructures for dye-sensitized solar cells.** *Adv Mater* 2009, **21:**4087.
3. Yu R, Lin QF, Leung SF, Fan ZY: **Nanomaterials and nanostructures for efficient light absorption and photovoltaics.** *Nano Energy* 2012, **1:**57.
4. Gibson EA, Smeigh AL, Pleux LL, Fortage J, Boschloo G, Blart E, Pellegrin Y, Odobel F, Hagfeldt A, Hammarström L: **A p-type NiO-based dye-sensitized solar cell with an open-circuit voltage of 0.35 V.** *Angew Chem Int Ed* 2009, **48:**4402.
5. Kinoshita T, Dy JT, Uchida S, Segawa TK: **Wideband dye-sensitized solar cells employing a phosphine-coordinated ruthenium sensitizer.** *Nat Photonics* 2013, **7:**535.
6. Yella A, Lee HW, Tsao HN, Yi CY, Chandiran AK, Nazeeruddin MK, Diau EWG, Yeh CY, Zakeeruddin SM, Grätzel M: **Porphyrin-sensitized solar cell with cobalt (II/III)-based redox electrolyte exceed 12 percent efficiency.** *Science* 2011, **334:**629.
7. Ji Z, Natu G, Huang Z, Wu Y: **Linker effect in organic door-accepter dyes for p-type NiO dye sensitized solar cells.** *Energy Environ Sci* 2011, **4:**2818.
8. Li L, Gibson EA, Qin P, Boschloo G, Gorlov M, Hagfeldt A, Sun LC: **Double-layered NiO photocathodes for p-type DSSCs with record IPCE.** *Adv Mater* 2010, **22:**1759.
9. Xiong DH, Xu Z, Zeng XW, Zhang WJ, Chen W, Xu XB, Wang MK, Cheng YB: **Hydrothermal synthesis of ultrasmall $CuCrO_2$ nanocrystal alternatives to NiO nanoparticles in efficient p-type dye-sensitized solar cells.** *J Mater Chem* 2012, **22:**24760.
10. Odobel F, Pellegrin Y: **Recent advances in the sensitization of wide-band-gap nanostructured p-type semiconductors. Photovoltaic and photocatalytic applications.** *J Phys Chem Lett* 2013, **4:**2551.
11. Powar S, Daeneke T, Ma MT, Fu D, Duffy NW, Götz G, Weidelener M, Mishra A, Bäuerle P, Spiccia L, Bach U: **Stable dye-sensitized solar cell electrolytes based on cobalt(II)/(III) complexes of a hexadentate pyridyl ligand.** *Angew Chem Int Ed* 2013, **52:**602.
12. Wang MK, Anghel AM, Marsan B, Ha NLC, Pootrakulchote N, Zakeeruddin SM, Grätzel M: **CoS supersedes Pt as efficient electrocatalyst for triiodide reduction in dye-sensitized solar cells.** *J Am Chem Soc* 2009, **131:**15976.
13. Wu MX, Lin X, Hagfeldt A, Ma TL: **A novel catalyst of WO_2 nanorod for the counter electrode of dye-sensitized solar cells.** *Chem Commun* 2011, **47:**4535.
14. Sun HC, Qin D, Huang SQ, Guo XZ, Li DM, Luo YH, Meng QB: **Dye-sensitized solar cells with NiS counter electrodes electrodeposited by a potential reversal technique.** *Energy Environ Sci* 2011, **4:**2630.
15. Jang JS, Ham DJ, Ramasamy E, Lee J, Lee LS: **Platinum-free tungsten carbides as an efficient counter electrode for dye sensitized solar cells.** *Chem Commun* 2010, **46:**8600.
16. Wu MX, Lin X, Hagfeldt A, Ma TL: **Low-cost molybdenum carbide and tungsten carbide counter electrodes for dye-sensitized solar cells.** *Angew Chem Int Ed* 2011, **50:**3520.
17. Zhou WJ, Wu XJ, Cao XH, Huang X, Tan CL, Tian J, Liu H, Wang JY, Zhang H: **Ni_3S_2 nanorods/Ni foam composite electrode with low overpotential for electrocatalytic oxygen evolution.** *Energy Environ Sci* 2013, **6:**2921.
18. Li ZQ, Gong F, Zhou G, Wang ZS: **NiS_2/reduced graphene oxide nanocomposites for efficient dye-sensitized solar cells.** *J Phys Chem C* 2013, **117:**6561.
19. Kung CW, Chen HW, Lin CY, Huang KC, Vittal R, Ho KC: **CoS acicular nanorod arrays for the counter electrode of an efficient dye-sensitized solar cell.** *ACS Nano* 2012, **6:**7016.
20. Xiao JW, Zeng XW, Chen W, Xiao F, Wang S: **High electrocatalytic activity of self-standing hollow $NiCo_2S_4$ single crystalline nanorod arrays towards sulfide redox shuttles in quantum dot-sensitized solar cells.** *Chem Commun* 2013, **49:**11734.
21. Li Y, Hasin P, Wu Y: **$Ni_xCo_{3-x}O_4$ nanowire arrays for electrocatalytic oxygen evolution.** *Adv Mater* 2010, **22:**1926.
22. Lin JY, Chou SW: **Highly transparent $NiCo_2S_4$ thin film as an effective catalyst toward triiodide reduction in dye-sensitized solar cells.** *Electrochem Commun* 2013, **37:**11.
23. Banerjee A, Upadhyay KK, Bhatnagar S, Tathavadekar M, Bansode U, Agarkar S, Ogale SB: **Nickel cobalt sulfide nanoneedle array as an effective alternative to Pt as a counter electrode in dye sensitized solar cells.** *RSC Advances* 2014, **4:**8289.
24. Shi ZW, Lu H, Liu Q, Deng KM, Xu LY, Zou RJ, Hu JQ, Bando Y, Golberg D, Li L: **$NiCo_2O_4$ nanostructures as a promising alternative for NiO in *p*-type dye-sensitized solar cells with high efficiency of 0.785%.** *Energy Technol* 2014, **2:**517.
25. Zhang G, Lou XW: **General solution growth of mesoporous $NiCo_2O_4$ nanosheets on various conductive substrates as high-performance electrodes for supercapacitors.** *Adv Mater* 2013, **25:**976.
26. Yuan C, Li J, Hou L, Zhang X, Shen L, Lou XW: **Ultrathin mesoporous $NiCo_2O_4$ nanosheets supported on Ni foam as advanced electrodes for supercapacitors.** *Adv Mater* 2012, **22:**4592.
27. Wang Q, Liu B, Wang X, Ran S, Wang L, Chen D, Shen GZ: **Morphology evolution of urchin-like $NiCo_2O_4$ nanostructures and their applications as pseudocapacitors and photoelectrochemical cells.** *J Mater Chem* 2012, **22:**21647.
28. Wang Q, Wang X, Liu B, Yu G, Hou X, Chen D, Shen GZ: **$NiCo_2O_4$ nanowire arrays supported on Ni foam for high-performance flexible all-solid-state supercapacitors.** *J Mater Chem A* 2013, **1:**2468.
29. Gong F, Wang H, Xu X, Zhou G, Wang ZS: **In situ growth of $Co_{0.85}Se$ and $Ni_{0.85}Se$ on conductive substrates as high-performance counter electrodes for dye-sensitized solar cells.** *J Am Chem Soc* 2012, **134:**10953.
30. Wang H, Sun K, Tao F, Stacchiola DJ, Hu YH: **3D honeycomb-like structured graphene and its high efficiency as a counter-electrode catalyst for dye-sensitized solar cells.** *Angew Chem Int Ed* 2013, **52:**9210.
31. Guai GH, Leiw MY, Ng CM, Li CM: **Sulfur-doped nickel oxide thin film as an alternative to pt for dye-sensitized solar cell counter electrodes.** *Adv Energy Mater* 2012, **2:**334.
32. Bai Y, Yu H, Li Z, Amal R, Lu GQ, Wang LZ: **In situ growth of a ZnO nanowire network within a TiO_2 nanoparticle film for enhanced dye-sensitized solar cell performance.** *Adv Mater* 2012, **24:**5850.
33. Ye MD, Zheng DJ, Lv MQ, Chen C, Lin CJ, Lin ZQ: **Hierarchically structured nanotubes for highly efficient dye-sensitized solar cells.** *Adv Mater* 2013, **25:**3039.
34. Gong F, Xu X, Li ZQ, Zhou G, Wang ZS: **$NiSe_2$ as an efficient electrocatalyst for a Pt-free counter electrode of dye-sensitized solar cells.** *Chem Commun* 2013, **49:**1437.

doi:10.1186/1556-276X-9-608
Cite this article as: Shi *et al.*: Efficient p-type dye-sensitized solar cells with all-nano-electrodes: $NiCo_2S_4$ mesoporous nanosheet counter electrodes directly converted from $NiCo_2O_4$ photocathodes. *Nanoscale Research Letters* 2014 **9**:608.